energies

MDPI

Article

Joint Planning Method of Shared Energy Storage and Multi-Energy Microgrids Based on Dynamic Game with Perfect Information

Qibo He [1], Changming Chen [2,*], Xin Fu [1], Shunjiang Yu [2], Long Wang [1] and Zhenzhi Lin [2]

[1] State Grid Wuxi Power Supply Company of Jiangsu Electric Power Co., Ltd., Wuxi 214061, China; heqb1@js.sgcc.com.cn (Q.H.); wx_fx@js.sgcc.com.cn (X.F.); wanglwx@js.sgcc.com.cn (L.W.)
[2] College of Electrical Engineering, Zhejiang University, Hangzhou 310027, China; yushunjiang@zju.edu.cn (S.Y.); linzhenzhi@zju.edu.cn (Z.L.)
* Correspondence: changmingchen@zju.edu.cn

Abstract: Under the background of the Energy Internet and the shared economy, it is of great significance to explore the collaborative planning strategies of multi-energy microgrids (MEMGs) and a shared energy storage operator (SESO) supported by shared energy storage resources. In this context, a joint planning method of SESO and MEMG alliances based on a dynamic game with perfect information is proposed in this paper. First, an upper-level model for energy storage capacity configuration and pricing strategy planning of SESO is proposed to maximize the total planning and operational income of SESO. Then, a lower-level model for the optimal configuration of MEMGs' alliance considering SES is proposed to minimize the total planning and operational costs of the MEMG alliance. On this basis, a solving algorithm based on the dynamic game theory with perfect information and the backward induction method is proposed to obtain the Nash equilibrium solution of the proposed bi-level optimization models. Finally, a case study with one SESO and an alliance consisting of five MEMGs is conducted, and the simulation results show that the proposed bi-level optimization method can increase SESO's net income by 1.47%, reduce the average planning costs for each MEMG at least by 1.7%, and reduce model solving time by 62.9% compared with other counterpart planning methods.

Keywords: shared energy storage; multi-energy microgrid; dynamic game with perfect information; optimal configuration; backward induction method

check for updates

Citation: He, Q.; Chen, C.; Fu, X.; Yu, S.; Wang, L.; Lin, Z. Joint Planning Method of Shared Energy Storage and Multi-Energy Microgrids Based on Dynamic Game with Perfect Information. *Energies* **2024**, *17*, 4792. https://doi.org/10.3390/en17194792

Academic Editor: Adrian Ilinca

Received: 24 July 2024
Revised: 16 September 2024
Accepted: 24 September 2024
Published: 25 September 2024

Copyright: © 2024 by the authors. Licensee MDPI, Basel, Switzerland. This article is an open access article distributed under the terms and conditions of the Creative Commons Attribution (CC BY) license (https://creativecommons.org/licenses/by/4.0/).

1. Introduction

In the background of the Energy Internet and the "dual carbon" goals, breaking the isolated system of traditional energy systems and constructing a multi-energy microgrid (MEMG) with multiple energy couplings has become a primary measure for governments and enterprises worldwide to promote energy transition [1]. Meanwhile, as an important energy technology with the capability of energy time shifting and spatiotemporal decoupling, energy storage plays a significant role in providing flexible regulation during the planning and construction of MEMGs [2]. Therefore, it is of great significance to explore the planning and construction strategies of MEMGs supported by energy storage resources [3].

Currently, many studies have focused on MEMG planning methods that take energy storage resources into account [4]. For example, a capacity planning model for MEMG energy conversion equipment and energy storage devices considering dynamic energy conversion efficiency coefficients is proposed in [5]. A capacity planning method for MEMG equipment is proposed in [6], which considers the investment constraints of energy conversion and storage devices to reduce the planning cost of MEMG. The energy hub modeling method of MEMG is improved using directed acyclic graph theory in [7], and based on this, a low-carbon capacity planning model for MEMG energy stations with

carbon capture devices and energy storage devices is proposed, aiming to minimize the total planning and operating cost of MEMG. An optimal planning method for hydrogen-based rural MEMG is proposed in [8], which considers multiple time scales and multi-energy storage devices, aiming to achieve economic and reliable carbon neutral energy supply in rural communities. A device location and capacity optimization method for MEMG is proposed in [9], which considers various energy facilities such as heat pumps, electrical energy storage, and thermal energy storage, aiming to reduce the overall planning cost of MEMG. In addition to the aforementioned physical energy storage, some studies have also explored planning methods for MEMG considering virtual energy storage. For example, the impact of demand response on the economic efficiency of MEMG equipment planning is analyzed in [10], and an optimal planning model for MEMG that considers demand response as virtual energy storage is proposed to reduce MEMG's total planning costs and carbon emissions. A two-stage robust optimization planning model for MEMG considering demand response is constructed in [11], and the optimal equipment configuration strategy for MEMG is obtained by iteratively optimizing the upper-level planning model and the lower-level operation model. A device capacity planning model for MEMG that considers virtual heat storage in heating networks is proposed in [12], and it is verified through case studies that virtual heat storage in heating networks can improve the economic efficiency of MEMG's planning while improving the consumption level of renewable energy. A coordinated siting and sizing model for MEMG considering generalized energy storage is established in [13], where the physical energy storage device and virtual heat energy storage are simultaneously considered in this paper to reduce the total planning and operating costs and carbon emissions.

The aforementioned studies focus on scenarios where energy storage is independently used by individual MEMGs. In these cases, the investment and operational costs of energy storage are relatively high, and the utilization rate of the equipment is relatively low, hindering the further development and application of energy storage in MEMGs. Shared energy storage (SES) is a new business model for energy storage that has emerged in the context of the current sharing economy, whose core idea is to temporarily transfer the usage rights of idle energy storage resources from energy storage owners to lessees for a certain fee. Under the background of the increasing renewable energy penetration, sharing energy storage among multiple MEMGs can effectively improve the economic efficiency of MEMG operations, the renewable energy consumption rate, and the utilization rate of energy storage devices. Since Qinghai province initiated China's first SES pilot in 2019, SES has gradually become a hot research topic in China's energy storage field in recent years. Against this background, some scholars have explored optimization planning methods for SES, aiming to improve the utilization rate and economic efficiency of energy storage devices. For example, a bi-level planning model for SES operators (SESOs) and users is constructed in [14], aiming to increase the revenue for both parties. An SES capacity planning model for wind farms and photovoltaic power stations in distribution networks is constructed in [15]. A business model in which SESOs provide ancillary services to renewable energy generators is proposed in [16], aiming to enhance the investment enthusiasm of SESOs. The abovementioned studies focus on large-scale centralized SES planning methods, some studies have also addressed optimization planning methods for distributed SES on the user side. For instance, an optimal configuration model for user-side SES under a peer-to-peer energy sharing framework is constructed in [17]. An optimal configuration method for electricity retailers is proposed in [18], which aims to reduce electricity procurement costs for retailers by analyzing the investment benefits of SES. An optimal configuration model for SES in communities with multiple buildings is proposed in [19], aiming to reduce the SES planning costs for communities. A community-oriented SES planning framework is proposed in [20], and the effectiveness of SES in reducing energy storage configuration costs is verified by case studies. In the context of the Energy Internet, some scholars have also explored planning methods for MEMGs considering SES. For example, a capacity planning model for SES jointly built by multiple

industrial MEMGs is constructed in [21], and the impact of SES on the economic efficiency of industrial MEMGs' planning under different capacity ratios is investigated. An SES planning and scheduling model for MEMG is established in [22], and a non-dominated sorting equilibrium optimizer algorithm is introduced to prevent the Pareto solution set from getting trapped in local optima and to guarantee the successful execution of the proposed benefit distribution mechanism.

The aforementioned studies have made significant contributions to the development of MEMG and SES, but the following shortcomings remain: (1) Most existing research focuses on the independent planning method of MEMG or SESO, with less attention paid to the collaborative planning of multiple MEMG alliances and SESO. In fact, the SES leasing and scheduling strategies of MEMG alliances are based on SESO's SES pricing, while the SES leasing strategies of MEMG alliances also affect SESO's physical storage planning, scheduling, and pricing strategies. Therefore, it is urgent to study the collaborative planning strategies of SESO and MEMG alliances. (2) Existing research on SES capacity planning mostly does not consider the impact of storage lifespan degradation. In reality, ignoring the degradation of storage lifespan may accelerate the depreciation of equipment residual value, thereby indirectly increasing SESO's planning costs. Thus, it is crucial to account for the impact of storage lifespan degradation in SESO's planning process.

Hence, a joint planning method of SESO and MEMG alliances based on a dynamic game with perfect information is proposed in this paper to address the abovementioned issues. The contributions of this paper are summarized as follows:

(1) An upper-level model for energy storage capacity configuration and pricing planning of SESO is proposed, aiming to maximize the total planning and operational income of SESO. Energy storage operation constraints that consider storage lifespan degradation are introduced to improve the lifespan of energy storage devices, thereby reducing SESO's energy storage configuration costs and subsequently increasing SESO's total planning income.

(2) A lower-level model for the optimal configuration of the MEMG alliance considering SES is proposed, aiming to minimize the total planning and operational costs of the MEMG alliance. In the lower-level model, each MEMG independently invests in ECDs, while jointly leasing and utilizing SES. The planning and operational costs of SES are allocated using the Shapley value method. Compared with the planning model where each MEMG independently invests in energy storage devices, the proposed lower-level model can achieve lower total planning and operational costs for the MEMG alliance.

(3) A solving algorithm based on the dynamic game theory with perfect information and the backward induction method is proposed to obtain the Nash equilibrium solution of the proposed bi-level optimization models. A dynamic non-cooperative game framework with a leader–follower hierarchical structure is constructed for the proposed bi-level optimization models. On this basis, the bi-level optimization model is iteratively solved using the dynamic game theory with perfect information, and the subgame perfect Nash equilibrium solution is obtained using the backward induction method. The most beneficial collaborative planning strategy for both SESO and the MEMG alliance can be obtained through the proposed solving algorithm.

2. Upper-Level Model for Energy Storage Capacity Configuration and Pricing Strategy Planning of SESO

The upper-level model is from the perspective of SESO, and reasonable strategies for SES capacity configuration electricity, charging and discharging, electricity purchasing and selling with the upper-level grid, and SES rental service pricing are formulated based on the SES leasing demand of MEMGs. It should be noted that the charging and discharging power of SES is transmitted through the distribution network, so SESO needs to pay a certain transmission fee to the distribution network.

The objective function of the upper-level model is to maximize SESO's net income, which is the SES service income over the planning period minus the physical energy storage investment cost, physical energy storage maintenance cost, and electricity trading cost with the grid company, as shown in Equation (1). It should be noted that the occurrence probability of scenario s, i.e., x^s, is introduced in the following Equation (1) to realize the modeling of the stochastic programming method, thereby dealing with uncertainty in the planning process:

$$F_{\mathrm{I}}^{\mathrm{U}} = \max \sum_{y=1}^{Y} \left[\begin{array}{l} \left(j_{\mathrm{SES,Cap}}^{\mathrm{MEMG}} C_{\mathrm{SES,Cap},y}^{\mathrm{MEMG}} + j_{\mathrm{SES,Pow}}^{\mathrm{MEMG}} C_{\mathrm{SES,Pow},y}^{\mathrm{MEMG}} \right) / (1+\delta)^y - \\ \left(j_{\mathrm{SES,Cap}}^{\mathrm{SESO}} C_{\mathrm{SES,Cap},y}^{\mathrm{SESO}} + j_{\mathrm{SES,Pow}}^{\mathrm{SESO}} C_{\mathrm{SES,Pow},y}^{\mathrm{SESO}} \right) / (1+\delta)^y - \\ 365 \sum_{s=1}^{S} \sum_{t=1}^{T} x^s j_{\mathrm{SES,main}}^{\mathrm{SESO}} \left(P_{\mathrm{SES,cha},y,s,t}^{\mathrm{SESO}} + P_{\mathrm{SES,dis},y,s,t}^{\mathrm{SESO}} \right) \Delta t / (1+\delta)^y - \\ 365 \sum_{s=1}^{S} \sum_{t=1}^{T} x^s \left(j_{y,s,t}^{\mathrm{EPC,buy}} P_{\mathrm{EPC,buy},y,s,t}^{\mathrm{SESO}} - j_{y,s,t}^{\mathrm{EPC,sell}} P_{\mathrm{EPC,sell},y,s,t}^{\mathrm{SESO}} \right) \Delta t / (1+\delta)^y \end{array} \right] \tag{1}$$

where Y, S, and T are the number of planning years, typical planning scenarios, and scheduling time, respectively; δ is the discount coefficient; $j_{\mathrm{SES,Cap}}^{\mathrm{MEMG}}$ and $j_{\mathrm{SES,Pow}}^{\mathrm{MEMG}}$ are the rental unit prices for the energy capacity and power capacity of the SES service used by MEMGs' alliance, respectively; $C_{\mathrm{SES,Cap},y}^{\mathrm{MEMG}}$ and $C_{\mathrm{SES,Pow},y}^{\mathrm{MEMG}}$ are the energy capacity and power capacity of SES rented by MEMGs' alliance from SESO at year y, respectively; $j_{\mathrm{SES,Cap}}^{\mathrm{SESO}}$ and $j_{\mathrm{SES,Pow}}^{\mathrm{SESO}}$ are the unit investment costs of the energy capacity and power capacity of the physical energy storage devices invested by SESO, respectively; $C_{\mathrm{SES,Cap},y}^{\mathrm{SESO}}$ and $C_{\mathrm{SES,Pow},y}^{\mathrm{SESO}}$ are the energy capacity and power capacity of the physical energy storage devices invested by SESO, respectively; $j_{\mathrm{SES,main}}^{\mathrm{SESO}}$ is the unit maintenance cost of the physical energy storage devices; $P_{\mathrm{SES,cha},y,s,t}^{\mathrm{SESO}}$ and $P_{\mathrm{SES,dis},y,s,t}^{\mathrm{SESO}}$ are the charging and discharging power of SESO's physical energy storage devices at time t in scenario s of year y, respectively; Δt is the interval between adjacent scheduling times; $j_{y,s,t}^{\mathrm{EPC,buy}}$ and $j_{y,s,t}^{\mathrm{EPC,sell}}$ are the unit price of electricity sales and repurchases by power grids at time t in scenario s of year y, respectively; and $P_{\mathrm{EPC,buy},y,s,t}^{\mathrm{SESO}}$ and $P_{\mathrm{EPC,sell},y,s,t}^{\mathrm{SESO}}$ are the power purchased from and sold to the grid company by SESO at time t in scenario s of year y, respectively.

In the upper-level model, a lifespan degradation model for physical energy storage devices is constructed based on the rainflow counting method, aiming to extend the lifespan of SES by limiting the daily charge–discharge cycle count, thereby indirectly reducing SESO's SES investment costs. The rainflow counting method is a commonly used analysis method in the field of material fatigue life research and is widely applied in engineering practice to analyze the relationship between discharge depth and lifespan of SES [23]. The rainflow counting method counts cycles based on the nonlinear relationship between the state of charge (SOC) of SES and scheduling times, thereby reflecting the relationship between discharge depth and lifespan of SES. Specifically, the steps to calculate the charge–discharge cycle count and discharge depth of SES within a scheduling period using the rainflow counting method are as follows:

First, the relationship curve between SOC and scheduling times of SES is rotated 90 degrees clockwise, assuming that the virtual rainflow starts to flow down from the initial point. Then, the rainflow drips vertically when it reaches each "eave", i.e., the peaks and valleys of SOC, until it falls to the next roof that is larger than the "peak eave" or smaller than the "valley eave", forming a charge–discharge cycle and recording the SOC values at the start and end points of the rainflow path. Next, the rainflow continues to flow down from the last charge–discharge cycle until it reaches the next "eave", repeating the abovementioned steps until it flows to the end of the scheduling period. Finally, based on each rainflow path and its start and end SOC values, the discharge depth of each rainflow path is calculated.

Taking the relationship curve between SOC and scheduling times of SES shown in Figure 1 as an example, it can be concluded according to the above steps that the first charge–

discharge cycle is B-C-B′, with a discharge depth of 16%; the second charge–discharge cycle is E-F-E′, with a discharge depth of 10%; the third partial charge–discharge cycle is A-B-B′-D, with a discharge depth of 58%; and the fourth partial charge–discharge cycle is D-E-E′-G, with a discharge depth of 40%.

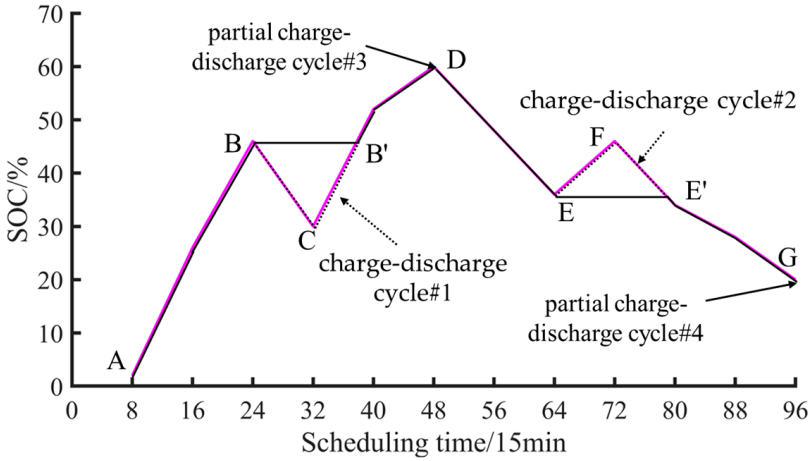


Figure 1. Relationship curve between SOC and scheduling times of SES.

Based on the abovementioned principles, it is evident that the process of calculating discharge depth and charge–discharge cycle count using the rainflow counting method involves solving nonconvex and nonlinear problems, such as extracting extreme values, which are challenging to express analytically. Therefore, the discharge level of ESD at each scheduling time is discretized in this paper, and equivalently converted into the maximum charge–discharge cycle count at a 100% discharge depth. By limiting the sum of the maximum charge–discharge cycle counts at each scheduling time within the scheduling period, a corresponding charge–discharge strategy of SES is formulated to reduce the degradation of SES lifespan. It should be noted that the depth of discharge of the ESD at each time step is normalized to a 100% depth of discharge. The reason is that the lifespan of the storage at a 100% depth of discharge is a standard for comparison. By converting the depth of discharge at each time step to a 100% depth of discharge, the following equations can be utilized to calculate the lifespan of the ESD at the current depth of discharge. The specific modeling steps are given below.

First, according to industry test data on the discharge depth and maximum charge–discharge cycle count of SES, a power function is used for curve fitting [24], deriving the relationship between the discharge depth and the maximum charge–discharge cycle count at the time, expressed as

$$N^{\mathrm{SESO}}_{\mathrm{SES,Life},y,s,t} = N_0 \left(d^{\mathrm{SESO}}_{\mathrm{SES,DOD},y,s,t} \Big/ \sum_{x=1}^{y} C^{\mathrm{SESO}}_{\mathrm{SES,Cap},x} \right)^{-k_p} \tag{2}$$

where $d^{\mathrm{SESO}}_{\mathrm{SES,DOD},y,s,t}$ is the actual discharge depth value of SES at time t; $N^{\mathrm{SESO}}_{\mathrm{SES,Life},y,s,t}$ is the number of charge–discharge cycles that SES can perform at discharge depth $d^{\mathrm{SESO}}_{\mathrm{SES,DOD},y,s,t}$ until reaching the maximum lifespan; N_0 is the number of charge–discharge cycles that SES can perform at a 100% discharge depth until reaching the maximum lifespan; and k_p is the fitting parameter.

Then, $N^{\mathrm{SESO}}_{\mathrm{SES,Life},y,s,t}$ is converted to the equivalent maximum cycle count $N^{\mathrm{SESO}}_{\mathrm{SES,eq},y,s,t}$ at a 100% discharge depth.

$$N^{\mathrm{SESO}}_{\mathrm{SES,eq},y,s,t} = \frac{N_0}{N^{\mathrm{SESO}}_{\mathrm{SES,Life},y,s,t}} = \left(d^{\mathrm{SESO}}_{\mathrm{SES,DOD},y,s,t} \Big/ \sum_{x=1}^{y} C^{\mathrm{SESO}}_{\mathrm{SES,Cap},x} \right)^{k_p} \tag{3}$$

Equation (3) is a nonconvex and nonlinear power function, making it difficult to construct a linear optimization model. Therefore, the power function is piecewise linearized in this section, as shown in Equation (4), with the addition of two constraints shown in Equations (5) and (6), as follows:

$$N^{\mathrm{SESO}}_{\mathrm{SES,eq},y,s,t} = \left(\frac{d^{\mathrm{SESO}}_{\mathrm{SES,DOD},y,s,t}}{\sum_{x=1}^{y} C^{\mathrm{SESO}}_{\mathrm{SES,Cap},x}}\right)^{k_p} = \left(\sum_{k=1}^{K} \frac{d^{\mathrm{SESO}}_{\mathrm{SES,DOD},y,s,t,k}}{\sum_{x=1}^{y} C^{\mathrm{SESO}}_{\mathrm{SES,Cap},x}}\right)^{k_p} \approx \sum_{k=1}^{K}\left[\left(K_{\mathrm{seg},k}\frac{d^{\mathrm{SESO}}_{\mathrm{SES,DOD},y,s,t,k}}{\sum_{x=1}^{y} C^{\mathrm{SESO}}_{\mathrm{SES,Cap},x}} + B_{\mathrm{seg},k}\right) g^{\mathrm{SESO}}_{\mathrm{SES},y,s,t,k}\right] \tag{4}$$

$$d_{\mathrm{DOD},k,\min} g^{\mathrm{SESO}}_{\mathrm{SES},y,s,t,k} \le d^{\mathrm{SESO}}_{\mathrm{SES,DOD},y,s,t,k} \le d_{\mathrm{DOD},k,\max} g^{\mathrm{SESO}}_{\mathrm{SES},y,s,t,k} \tag{5}$$

$$B^{\mathrm{SESO}}_{\mathrm{SES,cyc},y,s,t} = \sum_{k=1}^{K} g^{\mathrm{SESO}}_{\mathrm{SES},y,s,t,k} \tag{6}$$

where K is the number of linear segments; $K_{\mathrm{seg},k}$ and $B_{\mathrm{seg},k}$ are the slope and intercept of the k^{th} segment, respectively; $g^{\mathrm{SESO}}_{\mathrm{SES},y,s,t,k}$ is an auxiliary binary variable with a value of 1 indicating that the discharge depth of SES at time t in scenario s of year y falls within the k^{th} segment (thus, $d^{\mathrm{SESO}}_{\mathrm{SES,DOD},y,s,t,k} = d^{\mathrm{SESO}}_{\mathrm{SES,DOD},y,s,t}$), and a value of 0 indicating that the discharge depth does not fall within the k^{th} segment (thus, $d^{\mathrm{SESO}}_{\mathrm{SES,DOD},y,s,t,k} = 0$); $d_{\mathrm{DOD},k,\max}$ and $d_{\mathrm{DOD},k,\min}$ are the upper and lower bounds of the discharge depth for the k^{th} segment, respectively; and $B^{\mathrm{SESO}}_{\mathrm{SES,cyc},y,s,t}$ is an auxiliary binary variable reflecting the charge–discharge cycle status of SES at time t in scenario s of year y, with a value of 1 indicating the completion of a charge–discharge cycle at that time. It should be noted that, for Equation (4), according to the constraints shown in Equation (5), when $g^{\mathrm{SESO}}_{\mathrm{SES},y,s,t,k} = 0$, $d^{\mathrm{SESO}}_{\mathrm{SES,DOD},t,k} = 0$, and when $g^{\mathrm{SESO}}_{\mathrm{SES},y,s,t,k} = 1$, $d^{\mathrm{SESO}}_{\mathrm{SES,DOD},y,s,t,k} g^{\mathrm{SESO}}_{\mathrm{SES},y,s,t,k} = d^{\mathrm{SESO}}_{\mathrm{SES,DOD},y,s,t,k}$. Therefore, Equation (4) can be equivalently relaxed to Equation (7).

$$N^{\mathrm{SESO}}_{\mathrm{SES,eq},y,s,t} = \sum_{k=1}^{K}\left[K_{\mathrm{seg},k} d^{\mathrm{SESO}}_{\mathrm{SES,DOD},y,s,t,k} \Big/ \sum_{x=1}^{y} C^{\mathrm{SESO}}_{\mathrm{SES,Cap},x} + B_{\mathrm{seg},k} g^{\mathrm{SESO}}_{\mathrm{SES},y,s,t,k}\right] \tag{7}$$

Since the discharge depth $d^{\mathrm{SESO}}_{\mathrm{SES,DOD},y,s,t}$ of SES is a decision variable influenced by the energy storage charge–discharge strategy, it is subject to constraints related to SOC and the charge–discharge cycle status, as shown in (8) and (9). More specifically, Equation (8) represents the relationship between the discharge depth and SOC of SES; Equation (9) represents the relationship between the charge–discharge cycle status and the charge–discharge state, which indicates that a charge–discharge cycle is completed if and only if SES transitions from a discharge state to a charge state, as follows:

$$d^{\mathrm{SESO}}_{\mathrm{SES,DOD},y,s,t} = \left(\sum_{x=1}^{y} C^{\mathrm{SESO}}_{\mathrm{SES,Cap},x} - Q^{\mathrm{SESO}}_{\mathrm{SES},y,s,t-1}\right) B^{\mathrm{SESO}}_{\mathrm{SES,cyc},y,s,t} \tag{8}$$

$$B^{\mathrm{SESO}}_{\mathrm{SES,cha},y,s,t} - B^{\mathrm{SESO}}_{\mathrm{SES,cha},y,s,t-1} \le B^{\mathrm{SESO}}_{\mathrm{SES,cyc},y,s,t} \le \min\left\{B^{\mathrm{SESO}}_{\mathrm{SES,cha},y,s,t},\ 1 - B^{\mathrm{SESO}}_{\mathrm{SES,cha},y,s,t-1}\right\} \tag{9}$$

where $Q^{\mathrm{SESO}}_{\mathrm{SES},y,s,t-1}$ is the remaining energy capacity of SES at time $t-1$ in scenario s of year y, and $B^{\mathrm{SESO}}_{\mathrm{SES,cha},y,s,t}$ and $B^{\mathrm{SESO}}_{\mathrm{SES,cha},y,s,t-1}$ are auxiliary binary variables reflecting the charging state of SES at times t and $t-1$, respectively. For Equation (8), the big-M method can be employed to equivalently relax it into the following Equations (10) and (11):

$$0 \le d^{\mathrm{SESO}}_{\mathrm{SES,DOD},y,s,t} \le \sum_{x=1}^{y} C^{\mathrm{SESO}}_{\mathrm{SES,Cap},x} - Q^{\mathrm{SESO}}_{\mathrm{SES},y,s,t-1} \tag{10}$$

$$(\sum_{x=1}^{y} C_{\mathrm{SES,Cap},x}^{\mathrm{SESO}} - Q_{\mathrm{SES},y,s,t-1}^{\mathrm{SESO}}) - M(1 - B_{\mathrm{SES,cyc},y,s,t}^{\mathrm{SESO}}) \le d_{\mathrm{SES,DOD},y,s,t}^{\mathrm{SESO}} \le MB_{\mathrm{SES,cyc},y,s,t}^{\mathrm{SESO}} \quad (11)$$

where M is a positive real number with a sufficiently large numerical value.

Based on the aforementioned modeling, as long as the sum of the maximum charge–discharge cycle counts at each scheduling time is limited to within the maximum daily average charge–discharge cycle count derived from the expected lifespan of SES, SES can be effectively ensured to reach its expected lifespan, as shown in the following Equation (12):

$$\sum_{t=1}^{T} N_{\mathrm{SES,eq},y,s,t}^{\mathrm{SESO}} = \sum_{t=1}^{T}\sum_{k=1}^{K}\left(K_{\mathrm{seg},k} d_{\mathrm{SES,DOD},y,s,t,k}^{\mathrm{SESO}} / \sum_{x=1}^{y} C_{\mathrm{SES,Cap},x}^{\mathrm{SESO}} + B_{\mathrm{seg},k} g_{\mathrm{SES},y,s,t,k}^{\mathrm{SESO}}\right) \le N_{\mathrm{day}}^{\max} \quad (12)$$

where $N_{\mathrm{day}}^{\max}$ is the maximum daily average charge–discharge cycle count derived from the expected lifespan of SES, where $N_{\mathrm{day}}^{\max} = N_0 / N_{\mathrm{Life}}^{\mathrm{EXP}}$, $N_{\mathrm{Life}}^{\mathrm{EXP}}$ is the expected lifespan of SES.

For the nonlinear term in Equation (12), it can be converted to Equation (13) by multiplying both sides of the inequality by $\sum_{x=1}^{y} C_{\mathrm{SES,Cap},x}^{\mathrm{SESO}}$. Then, the product of binary and continuous variables, i.e., $g_{\mathrm{SES},y,s,t,k}^{\mathrm{SESO}} \sum_{x=1}^{y} C_{\mathrm{SES,Cap},x}^{\mathrm{SESO}}$, can be handled using the big-M method, thereby equivalently converting Equation (12) into a linear constraint.

$$\sum_{t=1}^{T} N_{\mathrm{SES,eq},y,s,t}^{\mathrm{SESO}} = \sum_{t=1}^{T}\sum_{k=1}^{K}\left(K_{\mathrm{seg},k} d_{\mathrm{SES,DOD},y,s,t,k}^{\mathrm{SESO}} + B_{\mathrm{seg},k} g_{\mathrm{SES},y,s,t,k}^{\mathrm{SESO}} \sum_{x=1}^{y} C_{\mathrm{SES,Cap},x}^{\mathrm{SESO}}\right) \le N_{\mathrm{day}}^{\max} \sum_{x=1}^{y} C_{\mathrm{SES,Cap},x}^{\mathrm{SESO}} \quad (13)$$

At this point, the energy storage lifespan degradation model based on the rainflow counting method has been constructed. Incorporating the basic operational constraints of SES shown in Equations (14)–(17) [25], they together form the operational constraints of SES considering lifespan degradation. More specifically, Equation (14) represents the constraint relationship between SOC and the charge–discharge power of SES; Equation (15) represents the constraint relationship between SOC and the invested energy capacity of SES; and Equations (16) and (17) represent the constraint relationships between the charge–discharge power and the invested power capacity of SES, as follows:

$$Q_{\mathrm{SES},y,s,t}^{\mathrm{SESO}} = Q_{\mathrm{SES},y,s,t-1}^{\mathrm{SESO}} + \delta_{\mathrm{cha}}^{\mathrm{SESO}} P_{\mathrm{SES,cha},y,s,t}^{\mathrm{SESO}} \Delta t - \delta_{\mathrm{dis}}^{\mathrm{SESO}} P_{\mathrm{SES,dis},y,s,t}^{\mathrm{SESO}} \Delta t \quad (14)$$

$$0 \le Q_{\mathrm{SES}}^{y,s,t} \le \sum_{x=1}^{y} C_{\mathrm{SES,Cap},x}^{\mathrm{SESO}} \quad (15)$$

$$0 \le P_{\mathrm{SES,cha},y,s,t}^{\mathrm{SESO}} \le \sum_{x=1}^{y} C_{\mathrm{SES,Pow},x}^{\mathrm{SESO}} \quad (16)$$

$$0 \le P_{\mathrm{SES,dis},y,s,t}^{\mathrm{SESO}} \le \sum_{x=1}^{y} C_{\mathrm{SES,Pow}}^{\mathrm{SESO}} \quad (17)$$

where $Q_{\mathrm{SES},y,s,t}^{\mathrm{SESO}}$ is the remaining energy capacity of SES at time t in scenario s of year y; $\delta_{\mathrm{cha}}^{\mathrm{SESO}}$ and $\delta_{\mathrm{dis}}^{\mathrm{SESO}}$ are the charging and discharging loss coefficients of SES, respectively; and $C_{\mathrm{SES,Cap}}^{\mathrm{SESO,max}}$ and $C_{\mathrm{SES,Pow}}^{\mathrm{SESO,max}}$ are the upper limits of the energy capacity and power capacity investment for SES, respectively.

The constraints of the upper-level model also include the upper and lower bound constraints of the rental pricing for the energy capacity and power capacity of SES, as shown in Equations (18) and (19), respectively; additionally, the constraint shown in Equation (20) represents that the SES charge–discharge demand of the MEMG alliance needs to be met, as follows:

$$j_{\mathrm{SES,Cap}}^{\mathrm{MEMG,min}} \le j_{\mathrm{SES,Cap}}^{\mathrm{MEMG}} \le j_{\mathrm{SES,Cap}}^{\mathrm{MEMG,max}} \quad (18)$$

$$j_{\mathrm{SES,Pow}}^{\mathrm{MEMG,min}} \le j_{\mathrm{SES,Pow}}^{\mathrm{MEMG}} \le j_{\mathrm{SES,Pow}}^{\mathrm{MEMG,max}} \quad (19)$$

$$\sum_{n=1}^{N}\left(P_{\mathrm{SES,cha},n,y,s,t}^{\mathrm{MEMG}}-P_{\mathrm{SES,dis},n,y,s,t}^{\mathrm{MEMG}}\right)=P_{\mathrm{SES,cha},y,s,t}^{\mathrm{SESO}}-P_{\mathrm{SES,dis},y,s,t}^{\mathrm{SESO}}+P_{\mathrm{EPC,sell},y,s,t}^{\mathrm{SESO}}-P_{\mathrm{EPC,buy},y,s,t}^{\mathrm{SESO}} \tag{20}$$

where $j_{\mathrm{SES,Cap}}^{\mathrm{MEMG,max}}$ and $j_{\mathrm{SES,Cap}}^{\mathrm{MEMG,min}}$ are the upper and lower bounds of the rental pricing for the energy capacity of SES set by SESO, respectively; $j_{\mathrm{SES,Pow}}^{\mathrm{MEMG,max}}$ and $j_{\mathrm{SES,Pow}}^{\mathrm{MEMG,min}}$ are the upper and lower bounds of the rental pricing for the power capacity of SES set by SESO, respectively; N is the number of MEMGs; and $P_{\mathrm{SES,cha},n,y,s,t}^{\mathrm{MEMG}}$ and $P_{\mathrm{SES,dis},n,y,s,t}^{\mathrm{MEMG}}$ are the charging and discharging power of the n^{th} MEMG at time t in scenario s of year y, respectively.

3. Lower-Level Model for Optimal Configuration of MEMGs' Alliance Considering SES

The lower-level model is designed from the perspective of MEMGs. Each MEMG independently plans its own ECDs based on its load demand and formulates its energy scheduling strategy. The MEMG alliance also develops a reasonable SES rental strategy. The following reasonable assumptions are made for the MEMG alliance: (1) The MEMG alliance needs to elect a representative to summarize the daily energy storage charge and discharge plans of each MEMG and notify SESO. (2) The MEMG alliance can rent SES services either annually or per planning period, based on negotiations between the MEMG alliance and SESO. In this paper, it is assumed that MEMGs rent SES services annually.

Each MEMG's energy supply sources include the electric power company (EPC), natural gas company (NGC), and distributed renewable energy sources (RES); the ECDs include electric heaters (EH), gas boilers (GB), and combined heat and power units (CHP); and the load types of MEMG include electric load and thermal load. Assuming that N MEMGs form an alliance to jointly use SES services, the objective function of the lower-level model, i.e., $F_{\mathrm{C}}^{\mathrm{L}}$, is to minimize the sum of the life cycle costs of each MEMG in the alliance, as shown in the following Equation (21):

$$F_{\mathrm{C}}^{\mathrm{L}}=\min\sum_{y=1}^{Y}\left[\begin{array}{l}\left(j_{\mathrm{SES,Cap}}^{\mathrm{MEMG}}C_{\mathrm{SES,Cap},y}^{\mathrm{MEMG}}+j_{\mathrm{SES,Pow}}^{\mathrm{MEMG}}C_{\mathrm{SES,Pow},y}^{\mathrm{MEMG}}\right)/(1+\delta)^{y}-\sum_{n=1}^{N}I_{\mathrm{ECD,res},n,y}^{\mathrm{MEMG}}/(1+\delta)^{Y-y}+\\ \sum_{n=1}^{N}\left(j_{\mathrm{EH}}^{\mathrm{MEMG}}C_{\mathrm{EH},n,y}^{\mathrm{MEMG}}+j_{\mathrm{GB}}^{\mathrm{MEMG}}C_{\mathrm{GB},n,y}^{\mathrm{MEMG}}+j_{\mathrm{CHP}}^{\mathrm{MEMG}}C_{\mathrm{CHP},n,y}^{\mathrm{MEMG}}\right)/(1+\delta)^{y}+\\ 365\sum_{n=1}^{N}\sum_{s=1}^{S}\sum_{t=1}^{T}x^{s}\left(j_{y,s,t}^{\mathrm{EPC,buy}}P_{\mathrm{EPC,buy},n,y,s,t}^{\mathrm{MEMG}}+j_{y,s,t}^{\mathrm{NGC,buy}}G_{\mathrm{NGC,buy},n,y,s,t}^{\mathrm{MEMG}}\right)\Delta t/(1+\delta)^{y}\end{array}\right] \tag{21}$$

where $I_{\mathrm{ECD,res},n,y}^{\mathrm{MEMG}}$ is the residual value of the ECDs invested by the n^{th} MEMG in year y [26]; $C_{\mathrm{EH},n,y}^{\mathrm{MEMG}}$, $C_{\mathrm{GB},n,y}^{\mathrm{MEMG}}$, and $C_{\mathrm{CHP},n,y}^{\mathrm{MEMG}}$ are the capacities of the newly built EH, GB, and CHP by the n^{th} MEMG in year y, respectively; $j_{\mathrm{EH}}^{\mathrm{MEMG}}$, $j_{\mathrm{GB}}^{\mathrm{MEMG}}$, and $j_{\mathrm{CHP}}^{\mathrm{MEMG}}$ are the unit capacity investment costs of EH, GB, and CHP, respectively; $j_{y,s,t}^{\mathrm{NGC,buy}}$ is the unit price of gas sold by the NGC at time t in scenario s of year y; and $P_{\mathrm{EPC,buy},n,y,s,t}^{\mathrm{MEMG}}$ and $G_{\mathrm{NGC,buy},n,y,s,t}^{\mathrm{MEMG}}$ are the power purchased from the EPC and the volume of gas purchased from the NGC by the n^{th} MEMG at time t in scenario s of year y, respectively.

The constraints of the lower-level model include the power balance constraints shown in Equations (22)–(24), the SES operational constraints shown in Equations (25)–(28), the ECD operational power upper limit constraint shown in Equation (29), and the energy conversion constraints shown in Equations (30)–(32), as follows:

$$P_{\mathrm{EPC,buy},n,y,s,t}^{\mathrm{MEMG}}+P_{\mathrm{CHP},n,y,s,t}^{\mathrm{MEMG}}+P_{\mathrm{RES},n,y,s,t}^{\mathrm{MEMG}}+P_{\mathrm{SES,dis},n,y,s,t}^{\mathrm{MEMG}}=P_{\mathrm{L},n,y,s,t}^{\mathrm{MEMG}}+P_{\mathrm{EH},n,y,s,t}^{\mathrm{MEMG}}+P_{\mathrm{SES,cha},n,y,s,t}^{\mathrm{MEMG}} \tag{22}$$

$$H_{\mathrm{CHP},n,y,s,t}^{\mathrm{MEMG}}+H_{\mathrm{EH},n,y,s,t}^{\mathrm{MEMG}}+H_{\mathrm{GB},n,y,s,t}^{\mathrm{MEMG}}=H_{\mathrm{L},n,y,s,t}^{\mathrm{MEMG}} \tag{23}$$

$$G_{\mathrm{NGC,buy},n,y,s,t}^{\mathrm{MEMG}}=G_{\mathrm{CHP},n,y,s,t}^{\mathrm{MEMG}}+G_{\mathrm{GB},n,y,s,t}^{\mathrm{MEMG}} \tag{24}$$

$$Q_{\mathrm{SES},n,y,s,t}^{\mathrm{MEMG}}=Q_{\mathrm{SES},n,y,s,t-1}^{\mathrm{MEMG}}+\delta_{\mathrm{cha}}^{\mathrm{MEMG}}P_{\mathrm{SES,cha},n,y,s,t}^{\mathrm{MEMG}}\Delta t-\delta_{\mathrm{dis}}^{\mathrm{MEMG}}P_{\mathrm{SES,dis},n,y,s,t}^{\mathrm{MEMG}}\Delta t \tag{25}$$

$$0 \le Q^{\mathrm{MEMG}}_{\mathrm{SES},n,y,s,t} \le C^{\mathrm{MEMG}}_{\mathrm{SES,Cap},n,y} \tag{26}$$

$$0 \le P^{\mathrm{MEMG}}_{\mathrm{SES,cha},n,y,s,t} \le C^{\mathrm{MEMG}}_{\mathrm{SES,Pow},n,y} \tag{27}$$

$$0 \le P^{\mathrm{MEMG}}_{\mathrm{SES,dis},n,y,s,t} \le C^{\mathrm{MEMG}}_{\mathrm{SES,Pow},n,y} \tag{28}$$

$$0 \le P^{\mathrm{MEMG}}_{E,n,y,s,t} \le \sum_{x=1}^{y} C^{\mathrm{MEMG}}_{E,n,x} \tag{29}$$

$$H^{\mathrm{MEMG}}_{\mathrm{CHP},n,y,s,t} = \eta^{\mathrm{H\text{-}G}}_{\mathrm{CHP}} G^{\mathrm{MEMG}}_{\mathrm{CHP},n,y,s,t} = \eta^{\mathrm{H\text{-}E}}_{\mathrm{CHP}} P^{\mathrm{MEMG}}_{\mathrm{CHP},n,y,s,t} \tag{30}$$

$$H^{\mathrm{MEMG}}_{\mathrm{EH},n,y,s,t} = \eta^{\mathrm{H\text{-}E}}_{\mathrm{EH}} P^{\mathrm{MEMG}}_{\mathrm{EH},n,y,s,t} \tag{31}$$

$$G^{\mathrm{MEMG}}_{\mathrm{GB},n,y,s,t} = \eta^{\mathrm{G\text{-}H}}_{\mathrm{GB}} H^{\mathrm{MEMG}}_{\mathrm{GB},n,y,s,t} \tag{32}$$

where $P^{\mathrm{MEMG}}_{\mathrm{L},n,y,s,t}$ and $H^{\mathrm{MEMG}}_{\mathrm{L},n,y,s,t}$ are the electric and thermal load powers of the n^{th} MEMG at time t in scenario s of year y, respectively; $P^{\mathrm{MEMG}}_{\mathrm{CHP},n,y,s,t}$ and $P^{\mathrm{MEMG}}_{\mathrm{RES},n,y,s,t}$ are the electric powers supplied by the CHP and the RES of the n^{th} MEMG at time t in scenario s of year y, respectively; $P^{\mathrm{MEMG}}_{\mathrm{EH},n,y,s,t}$ is the electric power consumed by the EH of the n^{th} MEMG at time t in scenario s of year y; $H^{\mathrm{MEMG}}_{\mathrm{CHP},n,y,s,t}$, $H^{\mathrm{MEMG}}_{\mathrm{EH},n,y,s,t}$, and $H^{\mathrm{MEMG}}_{\mathrm{GB},n,y,s,t}$ are the thermal powers supplied by the CHP, EH, and GB of the n^{th} MEMG at time t in scenario s of year y, respectively; $G^{\mathrm{MEMG}}_{\mathrm{CHP},n,y,s,t}$ and $G^{\mathrm{MEMG}}_{\mathrm{GB},n,y,s,t}$ are the natural gas consumption by the CHP and GB of the n^{th} MEMG at time t in scenario s of year y, respectively; $Q^{\mathrm{MEMG}}_{\mathrm{SES},n,y,s,t}$ and $Q^{\mathrm{MEMG}}_{\mathrm{SES},n,y,s,t-1}$ are the remaining energy capacities of SES leased by the n^{th} MEMG at time t in scenario s of year y, respectively; $P^{\mathrm{MEMG}}_{E,n,y,s,t}$ is the output power of ECDs, where $\boldsymbol{E}$ denotes CHP, GB, and EH; $C^{\mathrm{MEMG}}_{E,n,x}$ is the newly installed capacity of $\boldsymbol{E}$ of the n^{th} MEMG in year x; $C^{\mathrm{MEMG}}_{\mathrm{SES,Cap},n,y}$ and $C^{\mathrm{MEMG}}_{\mathrm{SES,Pow},n,y}$ are the energy capacity and power capacity leased by the n^{th} MEMG in year y for SES, respectively; $\eta^{\mathrm{H\text{-}E}}_{\mathrm{CHP}}$, $\eta^{\mathrm{H\text{-}G}}_{\mathrm{CHP}}$, $\eta^{\mathrm{H\text{-}E}}_{\mathrm{EH}}$, and $\eta^{\mathrm{G\text{-}H}}_{\mathrm{GB}}$ are the electrical-to-thermal conversion coefficient of CHP, electrical efficiency coefficient of CHP, thermal-to-electrical conversion coefficient of EH, and gas-to-thermal conversion coefficient of GB, respectively.

It should be noted that, after the lower-level model determines the ECD capacity planning and SES service leasing strategy for MEMGs within the planning period, the SES service leasing costs generated by the alliance during the planning period need to be reasonably allocated to maintain the stability of the alliance. The cooperative game theory points out that the differences in marginal benefits among alliance members will result in varying bargaining power during the cost-sharing process. Therefore, the marginal benefit contribution index is introduced in this section to assess the position of each MEMG in SES service cost-sharing negotiations. The Shapley value method achieves a fair distribution of SES service leasing costs generated by the alliance by measuring each MEMG's marginal benefit contribution in all potential sub-alliances. Hence, the SES service cost allocation result for the i^{th} MEMG in the coalition N, i.e., $C^{SV,SES}_{i,N}$, can be obtained by the Shapley value method, which is expressed as

$$C^{SV,SES}_{i,N} = \sum_{S \subset N} \frac{(|S|-1)!(n-|S|)!}{n!} \left(F^{\mathrm{L}}_{S-i} - F^{\mathrm{L}}_{S} \right) \tag{33}$$

where S is the potential sub-alliances in the MEMGs alliance N; $|S|$ is the number of MEMGs in S; F^{L}_{S} and F^{L}_{S-i} are the alliance income of the sub-alliance S and the sub-alliance $S-i$ (which excludes the i^{th} MEMG), respectively; and $F^{\mathrm{L}}_{S-i} - F^{\mathrm{L}}_{S}$ is the marginal benefit brought to the sub-alliance S by the joining of the i^{th} MEMG.

4. Solving Algorithm for Bi-Level Optimization Models Based on the Dynamic Game Theory with Perfect Information and the Backward Induction Method

For the previously constructed bi-level optimization model, the SES leasing and scheduling strategy of the MEMG alliance is based on SESO's SES pricing strategy. Therefore, SESO's SES pricing strategy indirectly affects each MEMG's ECD planning and scheduling strategy. Additionally, the SES leasing strategy of the MEMG alliance will also impact SESO's physical energy storage planning, scheduling, and pricing strategies. In summary, this process conforms to a dynamic non-cooperative game framework with a leader–follower hierarchical structure. Furthermore, the SES pricing strategy transmitted from the upper-level model to the lower-level model and the SES leasing and scheduling strategy feedback from the lower-level model are mutually public information. Therefore, the proposed joint planning bi-level optimization problem for SESO and MEMGs is a dynamic game with perfect information. In this context, a bi-level optimization model solving algorithm based on the dynamic game theory with perfect information and the backward induction method is proposed in this paper. More specifically, the bi-level optimization model is iteratively solved using the dynamic game theory with perfect information, and the subgame perfect Nash equilibrium solution of the bi-level optimization model is obtained using the backward induction method. The specific steps are as follows.

Let SESO be the leader and the MEMG alliance be the follower in the bi-level model, establishing a dynamic game with a perfect information framework, including the following elements: participants {SESO, MEMGs}, strategies $\{\boldsymbol{\beta}_{\mathrm{SESO}}^{\mathrm{PRICE}}, \boldsymbol{\beta}_{\mathrm{SESO}}^{\mathrm{I\&O}}, \boldsymbol{\beta}_{\mathrm{MEMG}}^{\mathrm{SES}}, \boldsymbol{\beta}_{\mathrm{MEMG}}^{\mathrm{I\&O}}\}$, and incomes $\{\gamma_{\mathrm{SESO}}^{\mathrm{PIDG}}, \gamma_{\mathrm{MEMG}}^{\mathrm{PIDG}}\}$. $\boldsymbol{\beta}_{\mathrm{SESO}}^{\mathrm{PRICE}}=\{p_{\mathrm{SES,Cap}}^{\mathrm{MEMG}}, p_{\mathrm{SES,Pow}}^{\mathrm{MEMG}}\}$ represents SESO's SES energy capacity and power capacity pricing strategies; $\boldsymbol{\beta}_{\mathrm{SESO}}^{\mathrm{I\&O}} = \{M_{\mathrm{SES,Cap},y}^{\mathrm{SESO}}, M_{\mathrm{SES,Pow},y}^{\mathrm{SESO}}, P_{\mathrm{SES,cha},y,s,t}^{\mathrm{SESO}}, P_{\mathrm{SES,dis},y,s,t}^{\mathrm{SESO}}, P_{\mathrm{EPC,buy},y,s,t}^{\mathrm{SESO}}, P_{\mathrm{EPC,sell},y,s,t}^{\mathrm{SESO}}\}$ ($y = 1, 2, \ldots, Y$; $s = 1, 2, \ldots, S$; $t = 1, 2, \ldots, T$) represents SESO's planning and scheduling strategies; $\boldsymbol{\beta}_{\mathrm{MEMG}}^{\mathrm{SES}} = \{M_{\mathrm{SES,Cap},y}^{\mathrm{MEMG}}, M_{\mathrm{SES,Pow},y}^{\mathrm{MEMG}}, P_{\mathrm{SES,cha},n,y,s,t}^{\mathrm{SESO}}, P_{\mathrm{SES,dis},n,y,s,t}^{\mathrm{SESO}}\}$ ($n = 1, 2, \ldots, N$; $y = 1, 2, \ldots, Y$; $s = 1, 2, \ldots, S$; $t = 1, 2, \ldots, T$) represents MEMGs' SES service usage and charge–discharge strategies; $\boldsymbol{\beta}_{\mathrm{MEMG}}^{\mathrm{I\&O}} = \{P_{\mathrm{EPC,buy},n,y,s,t}^{\mathrm{MEMG}}, G_{\mathrm{NGC,buy},n,y,s,t}^{\mathrm{MEMG}}, P_{\mathrm{CHP},n,y,s,t}^{\mathrm{MEMG}}, P_{\mathrm{RES},n,y,s,t}^{\mathrm{MEMG}}, P_{\mathrm{SES,dis},n,y,s,t}^{\mathrm{MEMG}}, P_{\mathrm{EH},n,y,s,t}^{\mathrm{MEMG}}, P_{\mathrm{SES,cha},n,y,s,t}^{\mathrm{MEMG}}, H_{\mathrm{GB},n,y,s,t}^{\mathrm{MEMG}}\}$ represents MEMGs' planning and scheduling strategies; and $\gamma_{\mathrm{SESO}}^{\mathrm{PIDG}} = F_{\mathrm{I}}^{\mathrm{U}}$ and $\gamma_{\mathrm{MEMG}}^{\mathrm{PIDG}} = -F_{\mathrm{C}}^{\mathrm{L}}$ represent the incomes for SESO and MEMGs, respectively.

When the follower makes an optimal response based on the leader's strategy, and the leader accepts this response without further changing its strategy, the dynamic game with perfect information reaches Nash equilibrium. Assuming that NE* = $\{\boldsymbol{\beta}_{\mathrm{SESO}}^{\mathrm{PRICE},*}, \boldsymbol{\beta}_{\mathrm{SESO}}^{\mathrm{I\&O},*}, \boldsymbol{\beta}_{\mathrm{MEMG}}^{\mathrm{SES},*}, \boldsymbol{\beta}_{\mathrm{MEMG}}^{\mathrm{I\&O},*}\}$ is the Nash equilibrium solution of the proposed bi-level model in this paper, it should satisfy the following conditions:

$$\begin{aligned} \mathrm{NE}^* &= \operatorname{argmax} \gamma_{\mathrm{SESO}}^{\mathrm{PIDG}}(\boldsymbol{\beta}_{\mathrm{SESO}}^{\mathrm{PRICE}}, \boldsymbol{\beta}_{\mathrm{SESO}}^{\mathrm{I\&O}}, \boldsymbol{\beta}_{\mathrm{MEMG}}^{\mathrm{SES},*}) \\ \text{s.t. } \left\{\boldsymbol{\beta}_{\mathrm{MEMG}}^{\mathrm{SES},*}, \boldsymbol{\beta}_{\mathrm{MEMG}}^{\mathrm{I\&O},*}\right\} &= \operatorname{argmin} \gamma_{\mathrm{MEMG}}^{\mathrm{PIDG}}(\boldsymbol{\beta}_{\mathrm{SESO}}^{\mathrm{PRICE},*}, \boldsymbol{\beta}_{\mathrm{MEMG}}^{\mathrm{SES}}, \boldsymbol{\beta}_{\mathrm{MEMG}}^{\mathrm{I\&O}}). \end{aligned} \tag{34}$$

According to the dynamic games theory with perfect information, the actions of participants are sequential, with the leader and follower making strategies in an interdependent manner in turn. The original dynamic game with perfect information can be broken down into a series of smaller subgame problems, making it easier to intuitively describe the sequence of actions, strategy information, and incomes of the game participants. Therefore, a game tree is used in this paper to illustrate the dynamic game process with perfect information. In the game tree, nodes representing sequential game actions are termed as nodes of the game tree, including initial nodes, decision nodes, and terminal nodes. It is evident that decision nodes can have multiple direct successor nodes, indicating that the participant at these decision nodes can choose from multiple strategies; terminal nodes indicate the end of the game and, thus, have no direct successors. Tracing back from a terminal node to its direct predecessor and repeating this process to the initial node, a

path in the game tree can be obtained, representing a combination of action plans among the participants.

The game tree of the dynamic game with perfect information for the proposed bi-level optimization model is shown in Figure 2. In Figure 2, decision node 1 represents SESO setting the energy capacity and power capacity pricing strategies of SES; based on the strategy from decision node 1, decision node 2 represents the MEMG alliance formulating the SES service usage and charge–discharge strategies, as well as the planning and scheduling strategies for each MEMG; decision node 3 represents SESO receiving the response from the MEMG alliance and then accordingly formulating its planning and scheduling strategies; the terminal node represents the final incomes for SESO and MEMGs based on the strategies from decision nodes 1–3. N_1, N_2, and N_3 denote the number of subgame nodes for decision nodes 1, 2, and 3, respectively.

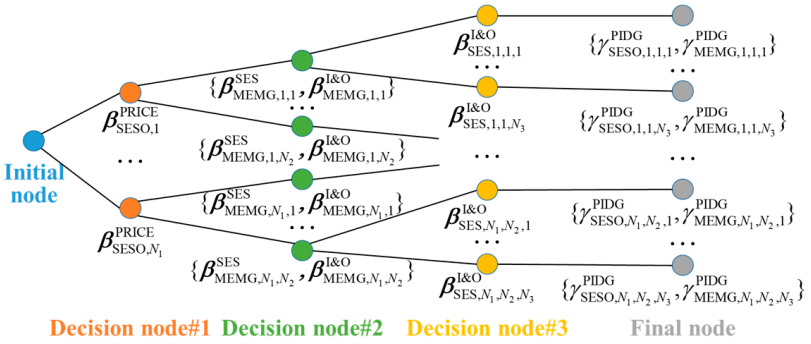


Figure 2. Game tree of the dynamic game with perfect information for the proposed bi-level optimization model.

Based on the aforementioned concepts, a subgame is defined as follows: Starting from a decision node in the game tree and including all subsequent nodes of that decision node, every decision node in the game tree can serve as an initial node, and together with all its subsequent nodes, they form a subgame. For the dynamic game with a perfect information problem of the proposed bi-level optimization model, if the strategy combination $\{\beta_{SESO}^{PRICE,*}, \beta_{SESO}^{I\&O,*}, \beta_{MEMG}^{SES,*}, \beta_{MEMG}^{I\&O,*}\}$ is the Nash equilibrium of the original dynamic game with a perfect information problem, and it is also the subgame Nash equilibrium for each subgame, then this strategy combination is called the subgame perfect Nash equilibrium (SPNE) of the proposed model [27]. Reference [28] has proven that a dynamic game with perfect information has a subgame perfect Nash equilibrium, and it has also proven that the backward induction method can be used to find the subgame perfect Nash equilibrium in a dynamic game with perfect information. Therefore, the backward induction method is employed in this paper to obtain the subgame perfect Nash equilibrium [29]. The backward induction method-based solving algorithm for the proposed bi-level optimization model is shown in Algorithm 1. The process of backward induction from a decision node to its direct predecessor can be solved using Gurobi 11.0 or CPLEX 12.9 commercial solvers.

Algorithm 1 Backward induction method-based solving algorithm for the proposed bi-level optimization model

Input: Parameters of the proposed bi-level optimization model in the first stage.
Initialize: i=1, j=1, k=1, S1flag_1=0, S1flag_2=0, S1flag _3=0, enter the initial node.
Repeat
    Enter decision node 1; the upper-level model provides the strategy $\beta^{\mathrm{PRICE}}_{\mathrm{SESO},i}$, and then transmits it to decision node 2.
    Repeat
        Enter decision node 2; the lower-level model provides the strategies $\beta^{\mathrm{SES}}_{\mathrm{MEMG},i,j}$ and $\beta^{\mathrm{I\&O}}_{\mathrm{MEMG},i,j}$, and then transmits it to decision node 3.
        Repeat
            Enter decision node 3; the upper-level model provides the strategy $\beta^{\mathrm{I\&O}}_{\mathrm{SESO},i,j,k}$, and then transmits the strategies $\{\beta^{\mathrm{PRICE}}_{\mathrm{SESO},i}, \beta^{\mathrm{SES}}_{\mathrm{MEMG},i,j}, \beta^{\mathrm{I\&O}}_{\mathrm{MEMG},i,j}, \beta^{\mathrm{I\&O}}_{\mathrm{SESO},i,j,k}\}$ to the terminal node.
            Enter the terminal node, solving the upper- and lower-level models proposed in Sections 2 and 3 to obtain $\{\gamma^{\mathrm{PIDG}}_{\mathrm{SESO},i,j,k}, \gamma^{\mathrm{PIDG}}_{\mathrm{MEMG},i,j,k}\}$.
        Backward induction to decision node 2, and according to (34), determine whether $\{\beta^{\mathrm{PRICE}}_{\mathrm{SESO},i}, \beta^{\mathrm{SES}}_{\mathrm{MEMG},i,j}, \beta^{\mathrm{I\&O}}_{\mathrm{MEMG},i,j}, \beta^{\mathrm{I\&O}}_{\mathrm{SESO},i,j,k}\}$ is the Nash equilibrium solution of the subgame tree starting at $\{\beta^{\mathrm{SES}}_{\mathrm{MEMG},i,j}, \beta^{\mathrm{I\&O}}_{\mathrm{MEMG},i,j}\}$. If it is, set S1flag_3=1; otherwise, set k=k + 1.
        Until $k > N_3$ or S1flag_3=1
    Backward induction to decision node 1, and according to (34), determine whether $\{\beta^{\mathrm{PRICE}}_{\mathrm{SESO},i}, \beta^{\mathrm{SES}}_{\mathrm{MEMG},i,j}, \beta^{\mathrm{I\&O}}_{\mathrm{MEMG},i,j}, \beta^{\mathrm{I\&O}}_{\mathrm{SESO},i,j,k}\}$ is the Nash equilibrium solution of the subgame tree starting at $\beta^{\mathrm{PRICE}}_{\mathrm{SESO},i}$. If it is, set S1flag_2=1; otherwise, set j=j + 1.
    Until $j > N_2$ or S1flag_2=1
Backward induction to initial node 1, and according to (34), determine whether $\{\beta^{\mathrm{PRICE}}_{\mathrm{SESO},i}, \beta^{\mathrm{SES}}_{\mathrm{MEMG},i,j}, \beta^{\mathrm{I\&O}}_{\mathrm{MEMG},i,j}, \beta^{\mathrm{I\&O}}_{\mathrm{SESO},i,j,k}\}$ is the Nash equilibrium solution of the initial game tree. If it is, set SPNE*=$\{\beta^{\mathrm{PRICE}}_{\mathrm{SESO},i}, \beta^{\mathrm{SES}}_{\mathrm{MEMG},i,j}, \beta^{\mathrm{I\&O}}_{\mathrm{MEMG},i,j}, \beta^{\mathrm{I\&O}}_{\mathrm{SESO},i,j,k}\}$, S1flag_1=1; otherwise, set i=i + 1.
Until $i > N_1$ or S1flag_1=1
Output: SPNE*
End

5. Case Studies

An example with one SESO and an alliance consisting of five MEMGs is used to validate the effectiveness of the proposed model. The topology of distribution and heating networks for each MEMG is shown in Figure 3, with a planning period of 10 years. The planning scenario curves during the planning period are shown in Figure 4, and the other parameters and scenario settings for the case are referenced from [30]. The proposed model is constructed in MATLAB R2023a using the Yalmip platform [31], and it is solved by the commercial solver GUROBI 11.0.

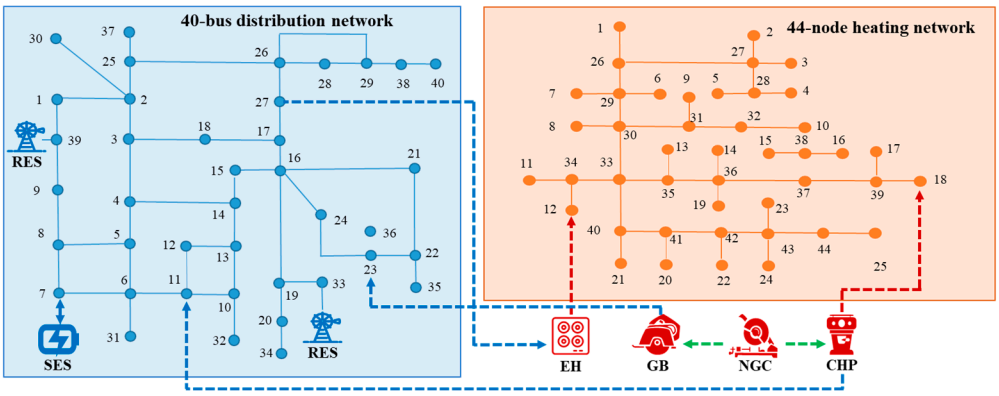


Figure 3. Topology of distribution and heating networks for each MEMG.

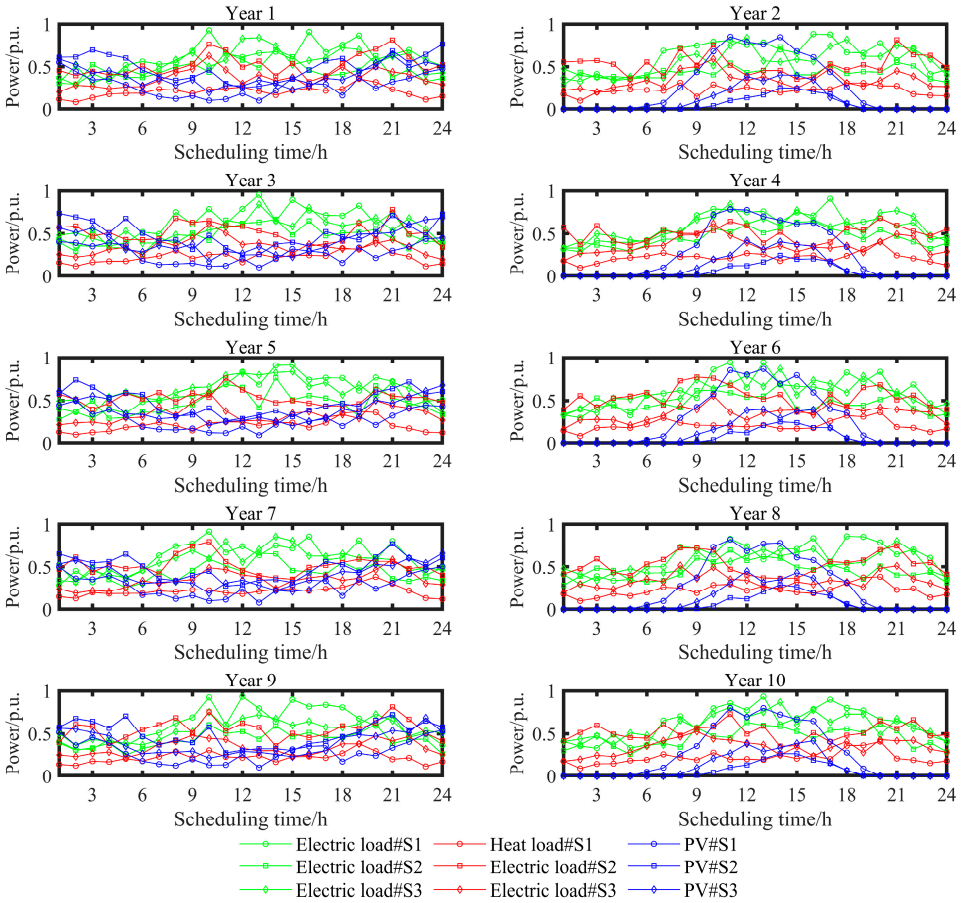


Figure 4. Planning scenario curves during the planning period.

5.1. Analysis for Planning and Scheduling Strategies of SESO

To analyze SESO's SES planning strategy, a comparison between the SES capacity invested by SESO and the SES leasing capacity of the MEMG alliance for each year of the planning period is shown in Figure 5. It can be seen from Figure 5 that SESO does not invest the entire SES capacity in the 1st year of the planning period. Instead, SESO invests SES capacity in the 4th, 5th, 7th, 8th, and 9th years based on the annual energy storage capacity leasing demand from MEMGs' alliance, thus maximizing SESO's income. It should be noted that the average SES energy capacity and power capacity invested by SESO each year during the planning period are 4.57 MWh and 2.82 MW, respectively, which are slightly less than the average SES energy capacity (5.09 MWh) and power capacity (3.84 MW) leased by the MEMG alliance each year during the planning period. This is because SESO can interact with the upper-level grid to reduce the capacity required for extreme SES usage scenarios, allowing SESO to invest slightly less SES capacity than what the MEMG alliance needs.

The annual costs for SESO over the planning period are shown in Table 1. It can be seen from Table 1 that the interaction costs between SESO and the power grid are positive in the 3rd and 8th–10th years, indicating that SESO's electricity purchasing costs from the power grid exceed its income from selling electricity to the power grid in these years; in other years, the income situation of SESO is opposite. This is because SESO's invested SES is charged and discharged rationally: when SES has idle energy and power capacity, its abundant electricity can be sold to the power grid for income, or electricity can be purchased from the power grid to meet high SES power demand from MEMGs' alliance at certain times. Additionally, SESO's annual SES service income varies because the demand for SES from the MEMG alliance changes as the capacity of ECDs invested by MEMGs increases. However, as more SES capacity is invested by SESO, the overall SES income increases. It should be noted that some SES energy capacities are invested

later, so the residual value of SES equipment at the end of the planning period remains at USD 181,000. This results in SESO achieving a total income of USD 482,000 over the entire planning period.

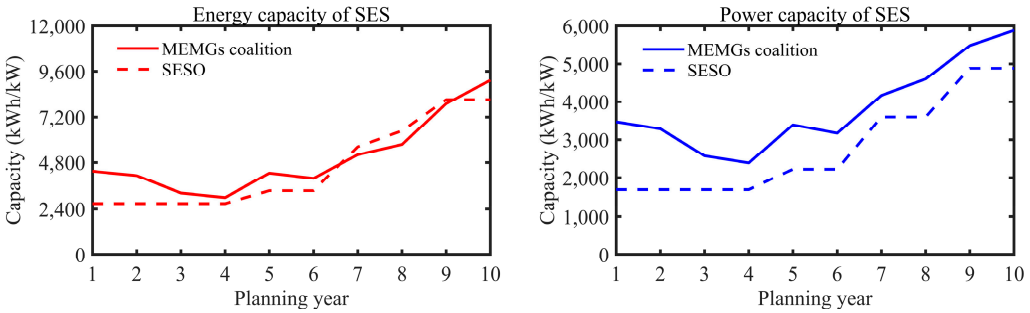


Figure 5. Comparison between the SES capacity invested by SESO and the SES leasing capacity of the MEMG alliance for each year of the planning period.

Table 1. Annual costs for SESO over the planning period (unit: USD 1×10^4).

Cost \ Year	1	2	3	4	5	6	7	8	9	10	Total
Investment cost of SES	32.7	0	0	0	6.2	0	17.3	4.5	11.4	0	72.3
Grid interaction cost	−2.2	−0.4	0.3	−0.2	−1.1	−1.2	−1.2	0.3	1.8	6.1	2.0
Equipment maintenance cost	0.3	0.2	0.3	0.3	0.3	0.3	0.3	0.3	0.5	0.6	3.8
SES income	13.6	11.9	8.6	7.4	9.8	8.4	10.3	10.5	13.2	14.0	108.2
SES residual value	0	0	0	0	0	0	0	0	0	18.1	18.1
Annual income	−17.1	12.1	8.0	7.4	4.3	9.4	−6.1	5.3	−0.5	25.3	48.2

To analyze the impact of considering energy storage lifespan degradation on improving the planning and operational economy of SESO in the upper-level optimization model, the cost comparison among the proposed model considering energy storage lifespan degradation (M-ESLD), the SESO planning model with fixed energy storage SOC limitation (M-FESSL) [26], and the SESO planning model without considering energy storage lifespan degradation (M-WESLD) [15] is shown in Table 2; a comparison of the SOCs of SES among M-WESLD, M-FESSL, and the proposed M-ESLD under different typical scheduling scenarios are shown in Figure 6. Combining the information from Table 2 and Figure 6, it can be seen that because M-WESLD does not consider constraints related to energy storage lifespan, its average discharge depth in various typical scheduling scenarios is 10.3% higher than that of the proposed M-ESLD, which allows M-WESLD to invest a smaller capacity of SES, resulting in SES investment costs that are USD 0.6×10^4 lower than those of the proposed M-ESLD. This also enhances SESO's scheduling flexibility to make M-WESLD's grid interaction costs USD 0.2×10^4 lower and SES income USD 1.8×10^4 higher than those of the proposed M-ESLD. However, because excessive discharge depth generates higher equipment maintenance costs and accelerates energy storage lifespan degradation, M-WESLD's equipment maintenance costs are USD 0.7×10^4 higher than those of the proposed M-ESLD, and its equipment residual value is also USD 2.6×10^4 lower than that of the proposed M-ESLD. In the M-FESSL, the SOC limits of SES are fixed within the range of 0.3 to 0.7. This constraint forces SESO to increase the investment cost by expanding the capacity of SES, i.e., USD 4.9×10^4 and USD 4.3×10^4 higher than that of the M-WESLD and the proposed M-ESLD, respectively. Furthermore, due to the significant reduction in the flexibility of SES scheduling, the grid interaction cost of the M-FESSL is 105.6% and 85.0% higher than that of the M-WESLD and M-ESLD, respectively. Although the limitation on the SES depth of discharge results in a 26.5% and 8.3% higher SES residual value under the M-FESSL compared with the M-WESLD and M-ESLD, respectively, the overall calculation shows that the annual income of SESO under the M-FESSL is the lowest among the three models, amounting to only USD 437,000. Overall, the proposed M-ESLD can replace

higher equipment residual value depreciation with lower planning and operating costs, and avoid the reduced scheduling flexibility of SES caused by artificially given discharge depths, resulting in 1.47% and 10.3% higher total incomes for SESO compared with the M-WESLD and M-FESSL.

Table 2. Cost comparison among the proposed M-ESLD, M-FESLD, and M-WESLD (unit: USD 1×10^4).

Cost / Model	Investment Cost of SES	Grid Interaction Cost	Equipment Maintenance Cost	SES Income	SES Residual Value	Annual Income
M-WESLD [15]	71.7	1.8	4.5	110.0	15.5	47.5
M-FESSL [26]	76.6	3.7	3.9	108.3	19.6	43.7
The proposed M-ESLD	72.3	2.0	3.8	108.2	18.1	48.2

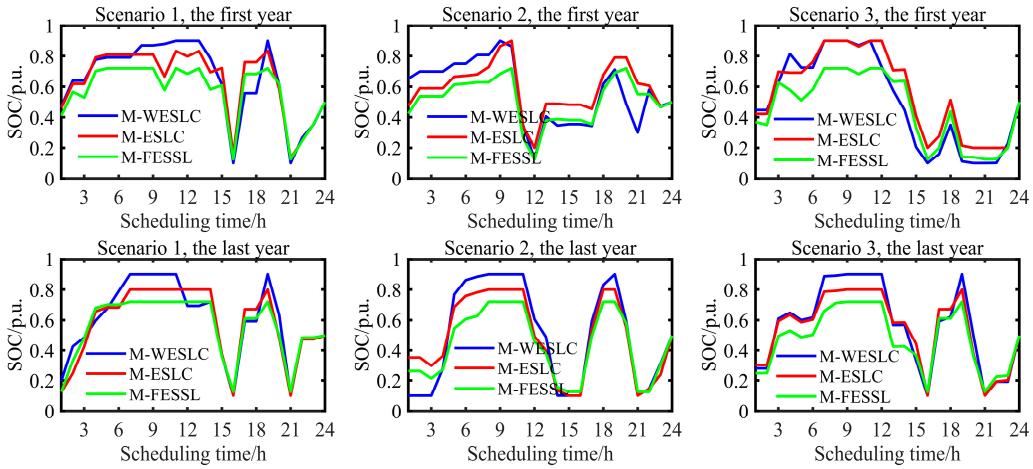


Figure 6. Comparison of the SOC of SES among the M-WESLD, the M-FESLD, and the proposed M-ESLD under different typical scheduling scenarios.

5.2. Analysis for Planning and Scheduling Strategies of MEMGs Alliance

The information presented in Table 3 includes the ECD investment capacity and SES leasing capacity for each MEMG in the MEMG alliance throughout the planning period. It can be seen from Table 3 that the ECD investment strategies vary among MEMGs due to differences in load types, quantities, and demands. For instance, MEMGs 1 and 5 invest in CHP annually in 1–9 years, whereas MEMGs 2–4 cease new CHP investments in 9–10 years. MEMG 2 invests in EH every year because it has a higher thermal load demand. As a result, the cumulative EH investment capacity of MEMG 2 is 4.48 MW, which is the highest among all MEMGs. It should be noted that EH is chosen over GB for heating equipment by all MEMGs. This preference arises from the cost comparison between generating 1 kWh of thermal power using $1/\eta_{\mathrm{EH}}^{\mathrm{H\text{-}E}}$ kWh of electricity and generating $1 \times \eta_{\mathrm{GB}}^{\mathrm{G\text{-}H}}$ cubic meters of natural gas, with the former being cheaper. For SES, the MEMG alliance opts for annual leasing from SESO instead of investing in physical energy storage devices. Consequently, the SES leasing capacity does not consistently increase but instead shows an initial decrease followed by an increase, reaching its lowest point in the 4th year with an SES energy capacity of 2986.7 kW and a power capacity of 2389.4 kW. By leasing SES energy and power capacities as needed, the planning costs of MEMGs' alliance can be reduced.

Table 3. ECD investment capacity and SES leasing capacity for each MEMG in the MEMG alliance throughout the planning period (unit: kW).

MEMG	Year	1	2	3	4	5	6	7	8	9	10
1	CHP	465.4	270.5	497.5	533.0	407.8	1011.9	751.3	615.0	121.1	0
	EH	2257.6	50.1	0	39.9	0	222.7	110.6	340.0	473.5	738.4
	GB	0	0	0	0	0	0	0	0	0	0
2	CHP	1100.2	226.1	389.7	437.0	353.9	690.5	602.7	650.7	0	0
	EH	1594.6	97.4	114.5	142.1	57.5	563.4	268.7	304.3	602.1	739.8
	GB	0	0	0	0	0	0	0	0	0	0
3	CHP	611.4	151.8	477.8	548.3	472.5	1110.2	682.9	358.0	0	0
	EH	1995.1	161.7	0	0	0	0	130.0	571.3	577.2	709.1
	GB	0	0	0	0	0	0	0	0	0	0
4	CHP	1225.0	263.4	423.9	469.4	340.9	815.9	716.0	529.1	0	0
	EH	1007.6	2.6	0	0	0	217.9	0	268.5	502.5	617.3
	GB	0	0	0	0	0	0	0	0	0	0
5	CHP	501.6	221.6	508.4	456.4	349.9	849.2	797.7	873.6	116.6	0
	EH	2031.0	78.5	0	31.8	31.5	305.5	0	0	437.0	687.7
	GB	0	0	0	0	0	0	0	0	0	0
SES	Energy	4338.8	4108.6	3219.1	2986.7	4239.5	3966.5	5209.5	5750.9	7901.8	9134.7
	Power	3471.0	3286.9	2575.2	2389.4	3391.6	3173.2	4167.6	4600.7	5481.2	5883.7

The SES charge–discharge scheduling strategy of the MEMG alliance in the first and last years of the planning period is shown in Figure 7. It can be seen from Figure 7 that, in the first year of the planning period, the SES usage frequency of each MEMG is relatively high due to the lower ECD capacities invested by the MEMG alliance. However, because the load demand of MEMGs in the first year is relatively low, the maximum charge–discharge power of SES is only 3471 kW, which is 41.0% lower compared with 5883 kW in the last year of the planning period. Additionally, it can also be seen from Figure 7 that, except for specific times such as hour 11 in scenario 2 of the first year, hour 10 in scenario 3 of the first year, and hour 17 in scenario 1 of the last year, where all five MEMGs simultaneously charge or discharge, there are complementary charge–discharge periods at other times. This allows the MEMG alliance to achieve the same optimized scheduling results with a lower SES investment capacity compared with each MEMG investing in individual energy storage devices, thereby reducing the planning and operational costs for each MEMG.

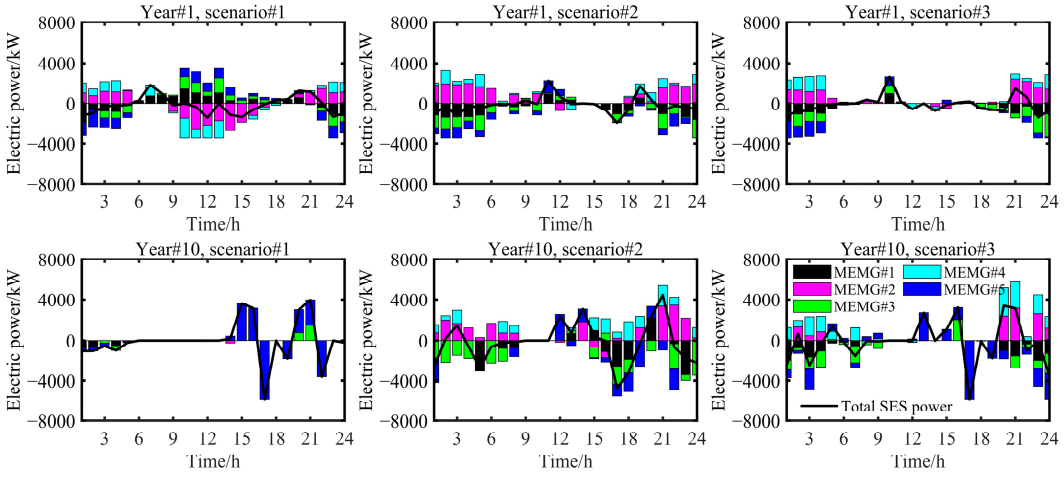


Figure 7. SES charge–discharge scheduling strategy of the MEMG alliance in the first and last years of the planning period.

To better validate the effectiveness of the MEMG alliance leasing SES in improving the economic efficiency of MEMG planning, a comparison of MEMG's planning costs of the planning model for MEMG considering self-built energy storage (M-SBES) [13], the planning model for MEMG lease SES from SESO individually (M-SES-I) [32], and the proposed planning model for MEMGs' alliance lease SES together (M-SES-A) is shown in Table 4. It can be seen from Table 4 that the planning costs for each MEMG in the M-SBES are the highest among the three models, followed by the M-SES-I, and the lowest in the proposed M-SES-A. This is because leasing SES can replace the high investment costs of physical energy storage with lower annual leasing costs, and this reduction in storage device investment costs is achieved while maintaining the same storage capacity. Consequently, the planning costs for each MEMG in the M-SES-I are at least USD 100,000 lower than those of the M-SBES. Based on the M-SES-I, the proposed M-SES-A further considers the MEMG alliance jointly leasing SES. As shown in Figure 7, the M-SES-A can utilize the complementary charge–discharge demands of different MEMGs to further reduce the leasing costs of SES. Additionally, it enables the MEMG alliance to leverage "economies of scale" in the dynamic game with perfect information against SESO. Therefore, the planning costs for each MEMG in the proposed M-SES-A are on average 1.7% lower than those of the M-SES-I.

Table 4. Comparison of MEMG's planning costs of the M-SBES, the M-SES-I, and the proposed M-SES-A.

Model	MEMG 1	MEMG 2	MEMG 3	MEMG 4	MEMG 5
M-SBES [13]	USD 8.9×10^6	USD 10.2×10^6	USD 8.8×10^6	USD 10.5×10^6	USD 8.6×10^6
M-SES-I [32]	USD 8.7×10^6	USD 9.9×10^6	USD 8.7×10^6	USD 10.2×10^6	USD 8.5×10^6
M-SES-A	USD 8.7×10^6	USD 9.8×10^6	USD 8.4×10^6	USD 10.1×10^6	USD 8.2×10^6

5.3. Analysis for the Dynamic Game with Perfect Information and the Solving Algorithm of the Proposed Bi-Level Optimization Model

The game tree of the proposed dynamic game with a perfect information problem based on the backward induction method is presented in Figure 8. In this game tree, the decision variables at decision node 1 are the energy capacity and power capacity leasing price of SES (unit: USD); the decision variables at decision node 2 are the SES energy capacity leased by MEMG, the SES power capacity leased by MEMG, the energy capacity of self-built storage by MEMG, and the power capacity of self-built storage by MEMG (units: MWh, MW, MWh, and MW, respectively); the decision variables at decision node 3 are the energy capacity and power capacity of SESO's invested storage (units: MWh and MW); the scalars at the terminal node are SESO's income and the MEMG alliance's costs (unit: USD 1×10^5). It can be seen from Figure 8 that when the SES service pricing is too low, such as USD 15 or USD 10, MEMGs do not build their own energy storage devices but instead lease higher capacities of SES services (4.68 MWh, 1.15 MW) to reduce their costs. In this case, the total planning and scheduling cost of the MEMG alliance is only USD 441.3×10^5. However, because the annualized price for SESO to invest in physical storage devices is higher than the annual leasing price of SES services, SESO's net income is negative, i.e., $-$USD 8.0×10^5. In such a scenario, SESO is dissatisfied with its income, and the subgame Nash equilibrium cannot be reached. When the SES leasing price is set at USD 18.0 or USD 16.9, SESO starts to gain positive income due to the increased pricing, achieving a subgame Nash equilibrium for the SES leasing price of USD 18.0 or USD 16.9. However, this is not the subgame perfect Nash equilibrium. If the SES service pricing is too high, such as USD 30.0 or USD 25.0), SESO's net income also decreases because the high SES service pricing reduces the MEMG alliance's demand for SES services, thereby decreasing SESO's income. When the SES service pricing is set at USD 26.6 or USD 15.5, it maximizes SESO's income while also prompting MEMGs' alliance to make optimal decisions. At this pricing, a subgame Nash equilibrium is achieved for an SES leasing price of USD 26.6 or

USD 15.5, which is also the subgame perfect Nash equilibrium in the dynamic game with a perfect information framework.

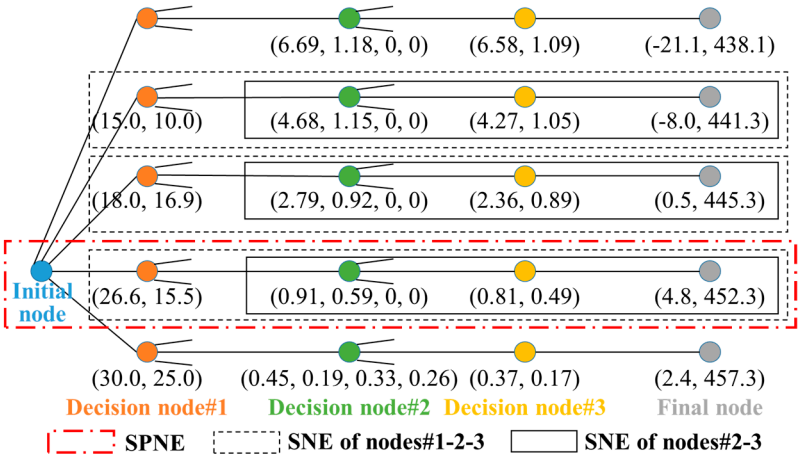


Figure 8. Game tree of the proposed dynamic game with a perfect information problem based on the backward induction method.

To validate the effectiveness of the proposed backward induction method-based solving algorithm (SA-BIM), a comparison among the proposed SA-BIM and other solving algorithms, i.e., the artificial intelligence-based solving algorithm [33] (SA-AI, using an improved genetic algorithm as an example, with both population size and number of iterations set to 200) and the marginal benefit-based solving algorithm [34] (SA-MB), is shown in Table 5. It can be seen from Table 5 that the SA-AI performs worse than the proposed SA-BIM in both solving time and solution quality. This is because artificial intelligence algorithms tend to fall into local optima and cannot realize parallel computations, resulting in longer solving times. The SA-MB finds the Nash equilibrium based on the marginal benefit increase or decrease in the SES pricing strategy, which has a higher mathematical theoretical basis compared with the SA-AI, but its convergence heavily depends on parameter settings, and improper parameter settings may lead to non-convergence. The proposed SA-BIM has the shortest solving time and can further improve solving efficiency through parallel computation. Additionally, the total income of the dynamic game's leader (SESO) is the highest. Therefore, the proposed SA-BIM provides the best solution and highest solving efficiency among the three algorithms.

Table 5. Comparison among the proposed SA-BIM, SA-AI, and SA-MB in terms of SESO income and solving time.

Index	The Proposed SA-BIM	SA-AI [33]	SA-MB [34]
SESO income	USD 4.82×10^5	USD 4.69×10^5	Depends on parameter setting
Solving time	7476 s	20,153 s	

6. Conclusions

A joint planning method of SESO and MEMG alliances based on a dynamic game with perfect information is proposed in this paper to realize the coordinated planning optimization between SESO and MEMG coalition. Case studies are conducted, and the following conclusions can be drawn:

(1) The proposed upper-level model for the energy storage capacity configuration and pricing planning of SESO can determine the most appropriate energy storage device investment strategy and energy scheduling strategy for SESO based on the SES usage demand of the MEMG alliance. By modeling energy storage lifespan degradation, the

proposed upper-level model can extend the lifespan of energy storage, thus increasing SESO's net income by 1.47% when compared with the counterpart planning model without considering energy storage lifespan degradation.

(2) The proposed lower-level model for the optimal configuration of MEMGs' alliance considering SES can obtain the optimal ECD configuration and scheduling strategy for each MEMG, as well as the optimal SES leasing and charge–discharge strategy for the MEMG alliance. The proposed lower-level model enables the MEMG alliance to leverage "economies of scale" in the dynamic game with perfect information against SESO. Therefore, the average planning costs for each MEMG in the proposed lower-level model are at least 1.7% lower than those for other MEMG planning models.

(3) The proposed solving algorithm for bi-level optimization models based on the dynamic game theory with perfect information and the backward induction method can find the subgame perfect Nash equilibrium solution for the proposed bi-level optimization model, ensuring that SESO and the MEMG alliance make optimal planning decisions. The proposed solving algorithm increases SESO income by 2.77% and reduces model solving time by 62.9% compared with other counterpart algorithms.

Author Contributions: Conceptualization, Q.H., C.C. and Z.L.; data curation, L.W. and S.Y.; formal analysis, L.W. and C.C.; funding acquisition, Q.H. and L.W.; investigation, L.W. and C.C.; methodology, X.F., S.Y. and Q.H.; project administration, X.F. and Z.L.; resources, X.F. and Z.L.; software, Q.H., S.Y. and X.F.; supervision, Z.L.; validation, C.C., S.Y. and Z.L.; visualization, L.W. and C.C.; writing—original draft, Q.H., S.Y. and X.F.; writing—review and editing, C.C., S.Y. and Z.L. All authors have read and agreed to the published version of the manuscript.

Funding: This study received funding from the Science and Technology Project of State Grid Jiangsu Electric Power Co., Ltd. (No. J2023083). The funder had the following involvement with the study: collection, analysis, interpretation of data.

Data Availability Statement: The original contributions presented in the study are included in the article.

Conflicts of Interest: Authors Qibo He, Xin Fu and Long Wang were employed by State Grid Wuxi Power Supply Company of Jiangsu Electric Power Co., Ltd. The remaining authors declare that the research was conducted in the absence of any commercial or financial relationships that could be construed as a potential conflict of interest.

References

1. Zhang, Y.; Sun, P.; Ji, X.; Wen, F.; Yang, M.; Ye, P. Low-carbon Economic Dispatch of Integrated Energy Systems Considering Extended Carbon Emission Flow. *J. Mod. Power Syst. Clean Energy*, 2024; *early access*. [CrossRef]
2. Kim, J.; Song, J.; Kim, C.; Mahseredjian, J.; Kim, S. Consideration on present and future of battery energy storage system to unlock battery value. *J. Mod. Power Syst. Clean Energy*, 2024; *early access*. [CrossRef]
3. Zhang, Y.; Li, J.; Ji, X.; Ye, P.; Yu, D.; Zhang, B. Optimal dispatching of electric-heat-hydrogen integrated energy system based on Stackelberg game. *Energy Convers. Econ.* **2023**, *4*, 267–275. [CrossRef]
4. Zhang, Y.; Lin, K.; Deng, W.; Zhang, D.; Xiao, D. A flexible voltage control strategy based on stage-division for microgrids. *Prot. Control Mod. Power Syst.* **2024**, *9*, 60–69. [CrossRef]
5. Mu, Y.; Chen, W.; Yu, X.; Jia, H.; Hou, K.; Wang, C.; Meng, X. A double-layer planning method for integrated community energy systems with varying energy conversion efficiencies. *Appl. Energy* **2020**, *279*, 115700. [CrossRef]
6. Wang, Y.; Li, R.; Dong, H.; Zhang, B.; Jiang, H.; Ding, C. Capacity planning and optimization of business park-level integrated energy system based on investment constraints. *Energy* **2019**, *189*, 116345. [CrossRef]
7. Dong, W.; Lu, Z.; He, L.; Li, Z.; Lin, W.; Wang, K. Low-carbon optimal planning of an integrated energy station considering combined power-to-gas and gas-fired units equipped with carbon capture systems. *Int. J. Electr. Power Energy Syst.* **2022**, *138*, 107966. [CrossRef]
8. Shao, Z.; Cao, X.; Zhai, Q.; Guan, X. Risk-constrained planning of rural-area hydrogen-based microgrid considering multiscale and multi-energy storage systems. *Appl. Energy* **2023**, *334*, 120682. [CrossRef]
9. Wang, J.; Deng, H.; Qi, X. Cost-based site and capacity optimization of multi-energy storage system in the regional integrated energy networks. *Energy* **2022**, *261*, 125240. [CrossRef]
10. Xiang, Y.; Cai, H.; Gu, C.; Zhang, Y.; Wang, H.; Li, X. Cost-benefit analysis of integrated energy system planning considering demand response. *Energy* **2020**, *192*, 116632. [CrossRef]

11. Yang, X.; Chen, Z.; Huang, X.; Liu, Y.; Li, Q.; Wang, F. Robust capacity optimization methods for integrated energy systems considering demand response and thermal comfort. *Energy* **2021**, *221*, 119727. [CrossRef]
12. Deng, X.; Huang, Y.; Chen, Y.; Li, J.; Zhang, P.; Li, Q. Multi-scenario physical energy storage planning of integrated energy systems considering dynamic characteristics of heating network and demand response. *Front. Energy Res.* **2021**, *9*, 783588. [CrossRef]
13. Chen, C.; Zhang, T.; Wang, Y.; Sun, G.; Wu, C.; Lin, Z. Coordinated siting and sizing for integrated energy system considering generalized energy storage. *Int. J. Electr. Power Energy Syst.* **2024**, *155*, 109619. [CrossRef]
14. Lai, S.; Qiu, J.; Tao, Y. Credit-based pricing and planning strategies for hydrogen and electricity energy storage sharing. *IEEE Trans. Sustain. Energy* **2022**, *13*, 67–80. [CrossRef]
15. Ma, M.; Huang, H.; Song, X.; Peña-Mora, F.; Zhang, Z.; Chen, J. Optimal sizing and operations of shared energy storage systems in distribution networks: A bi-level programming approach. *Appl. Energy* **2022**, *307*, 118170. [CrossRef]
16. Xu, X.; Li, G.; Yang, H.; Wang, H.; Zhang, S.; Xie, J. Pricing method of shared energy storage bias insurance service based on large number theorem. *J. Energy Storage* **2023**, *69*, 107726. [CrossRef]
17. Rodrigues, D.L.; Ye, X.; Xia, X.; He, H.; Li, M.; Zhang, J. Battery energy storage sizing optimisation for different ownership structures in a peer-to-peer energy sharing community. *Appl. Energy* **2020**, *262*, 114498. [CrossRef]
18. Liu, J.; Chen, X.; Xiang, Y.; Zhang, N.; Kang, C.; Kirschen, D. Optimal planning and investment benefit analysis of shared energy storage for electricity retailers. *Int. J. Electr. Power Energy Syst.* **2021**, *126*, 106561. [CrossRef]
19. Yang, Y.; Hu, G.; Spanos, C.J. Optimal sharing and fair cost allocation of community energy storage. *IEEE Trans. Smart Grid* **2021**, *12*, 4185–4194. [CrossRef]
20. Li, L.; Cao, X.; Zhang, S. Shared energy storage system for prosumers in a community: Investment decision, economic operation, and benefits allocation under a cost-effective way. *J. Energy Storage* **2022**, *50*, 104710. [CrossRef]
21. Zhang, Z.; Zhou, K.; Yang, S. Optimal selection of energy storage system sharing schemes in industrial parks considering battery degradation. *J. Energy Storage* **2023**, *57*, 106215. [CrossRef]
22. Dai, B.; Wang, H.; Li, B.; Li, C.; Tan, Z. Capacity model and optimal scheduling strategy of multi-microgrid based on shared energy storage. *Energy* **2024**, *306*, 132472. [CrossRef]
23. Andrenacci, N.; Chiodo, E.; Lauria, D.; Mottola, F. Life cycle estimation of battery energy storage systems for primary frequency regulation. *Energies* **2018**, *11*, 3320. [CrossRef]
24. Alharbi, H.; Bhattacharya, K. Stochastic optimal planning of battery energy storage systems for isolated microgrids. *IEEE Trans. Sustain. Energy* **2018**, *9*, 211–227. [CrossRef]
25. Zhang, W.; Xu, C. Capacity configuration optimization of photovoltaic-battery-electrolysis hybrid system for hydrogen generation consideringdynamic efficiency and cost learning. *Energy Convers. Econ.* **2024**, *5*, 78–92. [CrossRef]
26. Chen, C.; Zhu, Y.; Zhang, T.; Li, Q.; Li, Z.; Liang, H.; Liu, C.; Ma, Y.; Lin, Z.; Yang, L. Two-stage multiple cooperative games-based joint planning for shared energy storage provider and local integrated energy systems. *Energy* **2023**, *284*, 129114. [CrossRef]
27. Wang, C.; Hou, Y.; Ten, C. Determination of Nash equilibrium based on plausible attack-defense dynamics. *IEEE Trans. Power Syst.* **2017**, *32*, 3670–3680. [CrossRef]
28. Aliprantis, C.D. On the backward induction method. *Econ. Lett.* **1999**, *64*, 125–131. [CrossRef]
29. Wang, C.; Wang, Z.; Hou, Y.; Ma, K. Dynamic game-based maintenance scheduling of integrated electric and natural gas grids with a bilevel approach. *IEEE Trans. Power Syst.* **2018**, *33*, 4958–4971. [CrossRef]
30. Chen, C.; Li, Y.; Qiu, W.; Liu, C.; Zhang, Q.; Li, Z.; Lin, Z.; Yang, L. Cooperative-game-based day-ahead scheduling of local integrated energy systems with shared energy storage. *IEEE Trans. Sustain. Energy* **2022**, *13*, 1994–2011. [CrossRef]
31. Chen, C.; Wu, X.; Li, Y.; Zhu, X.; Li, Z.; Ma, J.; Qiu, W.; Liu, C.; Lin, Z.; Yang, L.; et al. Distributionally robust day-ahead scheduling of park-level integrated energy system considering generalized energy storages. *Appl. Energy* **2021**, *302*, 117493. [CrossRef]
32. Liu, J.; Zhang, N.; Kang, C.; Kirschen, D.; Xia, Q. Cloud energy storage for residential and small commercial consumers: A business case study. *Appl. Energy* **2017**, *188*, 226–236. [CrossRef]
33. Ali, K.B.; Telmoudi, A.J.; Gattoufi, S. Improved genetic algorithm approach based on new virtual crossover operators for dynamic job shop scheduling. *IEEE Access* **2020**, *8*, 213318–213329. [CrossRef]
34. Su, Z.; Xu, Q.; Fei, M.; Dong, M. Game theoretic resource allocation in media cloud with mobile social users. *IEEE Trans. Multimed.* **2016**, *18*, 1650–1660. [CrossRef]

Disclaimer/Publisher's Note: The statements, opinions and data contained in all publications are solely those of the individual author(s) and contributor(s) and not of MDPI and/or the editor(s). MDPI and/or the editor(s) disclaim responsibility for any injury to people or property resulting from any ideas, methods, instructions or products referred to in the content.